Available online at www.sciencedirect.com
SCIENCE DIRECT
Journal of the European Ceramic Society 26 (2006) 2627–2632
www.elsevier.com/locate/jeurceramsoc

Effect of calcination temperature on morphology of mesoporous YSZ

I-Ming Hung [a], De-Tsai Hung [a], Kuan-Zong Fung [a,*], Min-Hsiung Hon [a,b]

[a] *Department of Materials Science and Engineering, National Cheng Kung University, No. 1, Dashiue Road, Dung Chiu, Tainan 701, Taiwan*
[b] *Dayeh University, 112 Shan-Jiau Road, Da-Tsuen, Changhua 515, Taiwan*

Received 27 April 2005; received in revised form 21 July 2005; accepted 31 July 2005
Available online 10 October 2005

Abstract

A nano-structured mesoporous yttria-stabilized zirconia (YSZ) powders were prepared for the first time using cetyltrimethylammonium bromide (CTAB) as the surfactant and urea as the hydrolyzing agent and using $ZrO(NO_3)\cdot 6H_2O$ and $Y(NO_3)_3\cdot 6H_2O$ as inorganic precursors. The Brunauer–Emmett–Teller (BET) surface area, Barrett–Joyner–Halender (BJH) pore size distribution and crystallite/particle size of mesoporous YSZ varied with calcine temperatures were studied. Characterizations revealed that the mesoporous YSZ powder calcined at 600 °C was weakly agglomerated and had a high surface area of 137 m^2/g with an average grain size of ~5.8 nm. It was demonstrated that the mesoporous structure remained up to 900 °C. The low-densified YSZ sample with porosity as high as 33% was prepared from mesoporous YSZ powder sintered at 1500 °C for 6 h.

Keywords: Porosity; Surfactant; ZrO_2; Sintered; YSZ

1. Introduction

ZrO_2-based oxide is an important material due to its excellent chemical resistance, refractory character, oxygen ionic conductivity and polymorphous nature. It had been widely used for several practical applications, such as solid oxide fuel cells (SOFCs),[1] gas sensor[2,3] and automotive exhaust three-way catalysts.[4] In view of these applications, controlling the porosity of these systems is very important.

Since the discovery of the novel mesoporous silica by Kresge et al.,[5,6] much effort has been dedicated to exploiting their formation mechanism, surface modification and inclusion chemistry. Recently, a variety of mesoporous transition metal (TM) oxides[7] have been synthesized using the self-assemble of surfactant molecules as a template and applied on the promise applications, such as photovoltaic,[8] biochemical,[9] lithium-ion battery,[10] SOFC[11–14] and sensor.[15,16] However, the synthesis of mesoporous TM oxides is more difficult than that of silica-based materials, in view of the complexity of TM chemistry, such as their variable valence and coordination number, and high hydrolysis/condensation reactivity. In most cases, the mesoporous structure collapsed due to crystallization of metal-oxo during the subsequent calcination.[17–19]

Ozin and co-workers[20,21] were first to extend supramolecular template approach to the synthesis of mesoporous yttria-stabilized zirconia (YSZ) using cetyltrimethylammonium bromide ($[CH_3(CH_2)_{15}N^+(CH_3)_3Br^-]$, CTAB) as the template and using glycolate-modified inorganic solution as the metal ion precursors. Liu and co-workers[22] reported the preparation of mesoporous YSZ/NiO using Pluronic P103 as a structure-directing agent and inorganic chlorides as precursors in a nonaqueous medium. Gedanken and co-workers[23,24] reported that mesoporous YSZ was obtained when octanoic acid ($C_7H_{15}COOH$) was used as a templating agent and $Zr(i\text{-}OPr)_4$ and Y_2O_3 were used as metal ion sources. However, the morphology evolution of mesoporous YSZ with calcination temperature has not been investigated in detail.

SOFC based on anode supported structure and a dense thin-film electrolyte can be operated at intermediate temperature and yet achieve high power density as demonstrated by Souza[25] and Virkar.[26] Most of thin-film type cells are supported by porous anode. Among various processes developed for fabricating high

* Corresponding author. Tel.: +886 6 2380208; fax: +886 6 2380208.
E-mail address: kzfung@mail.ncku.edu.tw (K.-Z. Fung).

0955-2219/$ – see front matter © 2005 Elsevier Ltd. All rights reserved.
doi:10.1016/j.jeurceramsoc.2005.07.069

porous anode, graphite or polymer was added as the porous former. However, it is difficult to homogeneously mixture the porous former and ceramic powders due to the density difference. It is therefore of great practical importance to prepare the porous anode without adding porous former. Up to now, control of porosity and morphology of anode after sintering at high temperature is still one of the challenges for SOFC anode.

In this study, urea is used as a precipitating agent to promote a uniform base condition that avoid localized precipitation which gives wide particle size distribution, as well as a slow polymerization. The decomposition reaction is a function of temperature and expressed as following[27]:

$$(H_2N)_2CO + 3H_2O \rightarrow CO_2 + 2OH^- + 2NH_4^+ \quad (1)$$

The CTAB surfactant is used as the template for preparing mesoporous YSZ. The purpose of the present work is: (i) to investigate the morphology evolution and crystallite growth at the nano-level of the mesoporous YSZ powders as a function of calcination temperature; (ii) to prepare highly porous YSZ with open channels which may be suitably used as the anode support for SOFC.

2. Experimental

In this method, cetyltrimethylammonium bromide (CTAB, Fluka, 99%) was used as surfactant template, urea (J.T. Baker, 99%) was used as the precipitant agent and the $ZrO(NO_3)\cdot 6H_2O$ (Aldrich, 99.9%) and $Y(NO_3)_3\cdot 6H_2O$ (Alfa, 99.9%) were used as sources of zirconium and yttrium ions, respectively. The molar ratio of Y/Zr was 1/2, and the molar ratio of (Y + Zr)/CTAB/urea was 1/4.06/43.48. Typically, 1.672 g $ZrO(NO_3)\cdot 6H_2O$ and 0.780 g $Y(NO_3)_3\cdot 6H_2O$ were dissolved in 100 ml de-ionized water. Subsequently, 9.891 g CTAB and 18 g urea were added and stirred for 1 h. The precipitate reaction was employed at 80 °C for 6 h and the suspension was filtered and dried at 60 °C for 12 h. Finally, the products were calcined at various temperatures from 600 to1200 °C for 4 h.

Thermogravimetric analysis (TGA) was carried out using Setaram, Setsys Evolution Version 16 instrument. The sample was heated with a rate of 10 °C/min from 25 to 800 °C in air. The phase identification was performed by X-ray diffraction (XRD) using a Rigaku, Model Rad II diffractometer with Cu Kα radiation (λ = 1.5406 Å) and Ni filter, operated at 30 kV, 20 mA. Lattice constants were determined by a least-squares refinement of the d-spacing, which were measured in comparison with an internal standard of pure Si. The crystallite size of the calcined powders was calculated by the X-ray line broadening technique performed on the (1 1 1) diffraction of YSZ using Scherrer equation[28]:

$$D_{XRD} = \frac{(0.9\lambda)}{(\beta \cos\theta)} \quad (1)$$

where D_{XRD} is the crystallite size (nm), λ is the radiation wavelength (0.15406 nm), θ is the diffraction peak angle and β is the corrected half-width at half-maximum intensity (FWHM) given by:

$$\beta^2 = \beta_m^2 - \beta_s^2 \quad (2)$$

where β_m is the measured FWHM and β_s is the FWHM of a standard YSZ sample which was prepared by solid state reaction method. The nitrogen adsorption/desorption isotherms and specific surface area were performed by Micromeritics ASAP 2010 instrument at 77 K. The measured specific surface areas were converted to equivalent particle size according to the following equation:

$$D_{BET} = \frac{6 \times 10^3}{(\rho S_{BET})} \quad (3)$$

where D_{BET} (nm) is the average particle size, S_{BET} is the specific surface area expressed in m^2/g, ρ is the theoretical density of YSZ expressed in g/cm^3. The morphology of calcined powders was carried out by transmission electron microscopy (TEM, Model HF-200, Hitachi, Japan). The samples for TEM were prepared by dispersing the calcined powders in carbon-copper grids.

In order to further investigate the high temperature behavior of this mesoporous YSZ powders, disk-shaped samples of 8 mm diameter and 1 mm thickness were prepared by cold isotropic pressing (CIP) at 250 MPa. Subsequently, the sample was sintered at 1500 °C for 6 h.

3. Results and discussion

Thermogravimetric analysis of YSZ precursor consisting of CTAB surfactant, urea and nitrates is shown in Fig. 1. The initial weight loss occurring between 25 and 100 °C corresponds to the removal of residual water. The weight loss observed between 150 and 250 °C was caused by the elimination of the trimethylamine head group, via Hofmann degradation, which lead to a hydro-

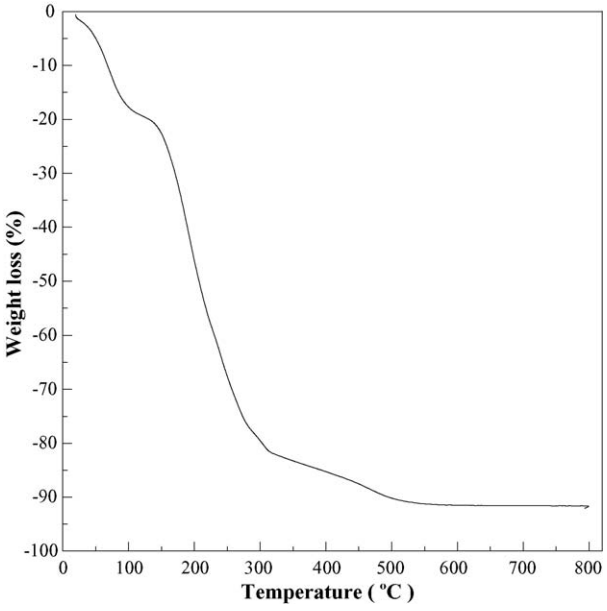

Fig. 1. The TGA curve of YSZ precursor with heating rate of 10 °C/min.

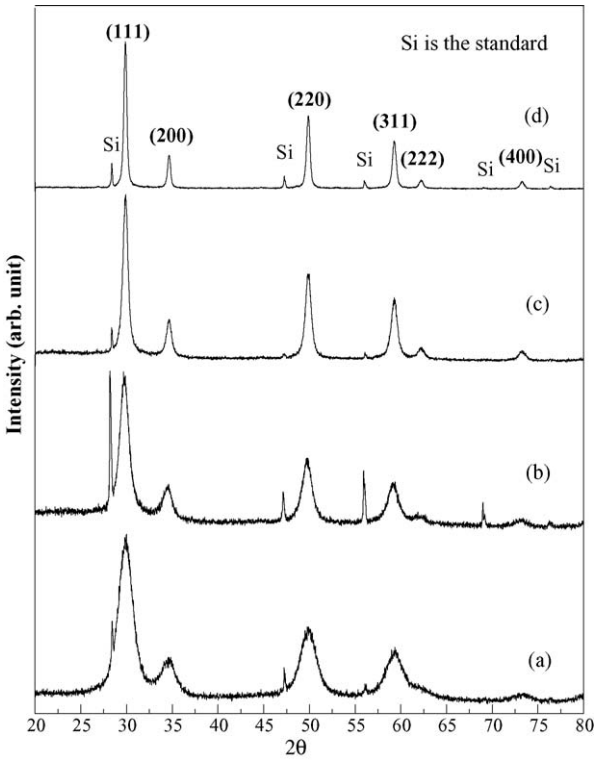

Fig. 2. The XRD patterns of YSZ powders calcined at (a) 600 °C; (b) 800 °C; (c) 1000 °C; and (d) 1200 °C.

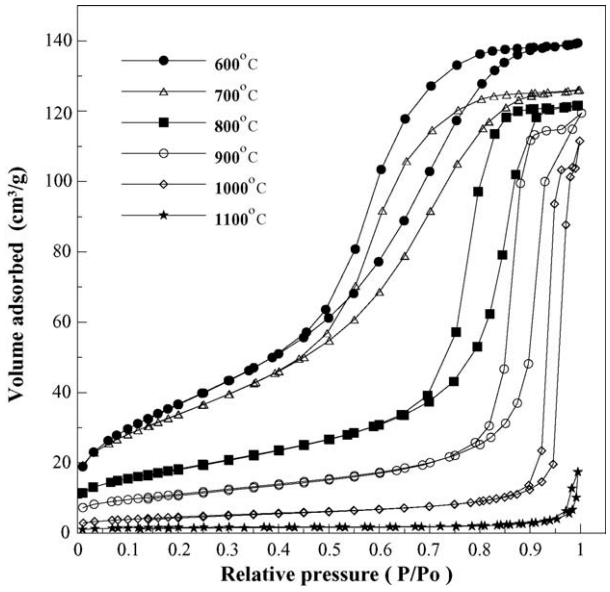

Fig. 3. Nitrogen adsorption/desorption isotherms of YSZ powders calcined at various temperatures.

carbon chain. The weight loss between 250 and 300 °C resulted from a successive carbon chain fragmentation or decomposition with early oxidation of different fragments.[29] Some cracking reactions on the hydrocarbon chain might occur as well. Finally, the weight loss, between 300 and 500 °C, was caused by the removal of the remaining organic constituents. From the TGA analysis, it was known that the template may be removed completely above 500 °C. Thus, the thermal stability of mesoporous YSZ was investigated at calcination temperatures above 600 °C in this study.

The XRD patterns, as shown in Fig. 2, of samples calcined at various temperatures indicate that mainly the cubic phase of YSZ (JCPDS no. 77-2112) was present. The line broadening in the XRD pattern indicated that the powder consists of nanocrystallites. The decrease in the FWHM of peaks with increasing calcination temperature indicates an increase in the YSZ nanocrystallite size as the calcination temperature increased. The lattice parameter for all samples is ~5.15 Å which implies that the yttrium ion completely dissolved in zirconia structure above 600 °C and the cubic structure was stabilized to room temperature. The stabilization mechanism can be traced from the following defect reaction:

$$Y_2O_3 \xrightarrow[ZrO_2]{} 2Y'_{Zr} + V_o^{\bullet\bullet} + 3O_O^x \quad (3)$$

Based on this reaction, the addition of Y_2O_3 into ZrO_2 was able to increase the average cationic radius because r_{Y3+} (1.019 Å, coordination number, CN = 8) is greater than that of r_{Zr4+} (0.84 Å, CN = 8) and enhance the concentration of oxygen vacancies. Consequently, cubic ZrO_2 was fully stabilized to room temperature by the addition of Y_2O_3.

The BET surface area, crystallite and particle size of samples calcined at various temperatures are shown in Table 1. The $\psi = (D_{BET}/D_{XRD})^3$ as a factor to reflect the partial sintering extent of the primary crystallites.[31] The crystallite size of sample calcined at 600 °C was calculated to be 5.8 nm according to the Scherrer equation. The measured BET surface area is 137 m^2/g, which is equivalent to a particle size of 7.5 nm. The

Table 1
Crystallite/particle size of the YSZ powders calcined at various temperatures

Calcination temperature (°C)	S_{BET} (m^2/g)	Pore size (nm)	Crystallite/particle size (nm)		
			D_{XRD}	D_{BET}	ψ
600	137	5	5.8	7.5	2.2
700	124	5	7.3	8.3	1.5
800	66	14	10.0	15.7	3.8
900	40	23	16.2	25.9	4.1
1000	17	43	26.6	60.8	12.0
1100	5.9	–	41.2	175.3	77.3
1200	3.3	–	47.2	313.4	292.6

D_{XRD} is crystallite size determined via XRD. D_{BET} is particle size determined by BET. $\Psi = (D_{BET}/D_{XRD})^3$.

crystallite size (D_{XRD}) determined via XRD and the particle size (D_{BET}) determined via BET data show small discrepancies below 700 °C, indicating that the primary crystallites are essentially non-partial sintering. As the samples calcined at 800 and 900 °C, ψ value is 3.8 and 4.1, respectively, which meant that the powers are light-partial sintering. Above 1000 °C, the difference between D_{BET} and D_{XRD} is apparently enlarged. The ψ value apparently increased to 292.6, indicating that the powders were virtually hard-sintered. From the above-mentioned results, crystallite growth may be divided into three different ranges between 600 and 1200 °C. In the temperature range of 600–700 °C, where the mesoporous structure still remain intact, the crystallite growth was slow and the BET surface area remained as high as 137 and 124 m^2/g, respectively. The low crystallite growth implied that the growth of crystallite is less dependent on the temperature and may be suppressed by the presence of mesopores which act as the second phase and prohibits the growth of crystallite.[15] In the temperature range of 700–900 °C, when the pores gradually collapsed and the crystallite was able to grow faster without the inhibition of meso-pores. At temperature greater than 900 °C, the subsequent sintering occurred. That is the reason why the particle size is larger than the crystallite size and the BET surface area apparently decreased.

The adsorption/desorption isotherms and BJH pore size distribution of mesoporous YSZ calcined at various temperatures are shown in Figs. 3 and 4, respectively. The isotherm for the mesoporous YSZ calcined at 600 °C exhibits distinct hysteresis loop in the P/Po ranging from 0.4 to 0.9, which is the typical characteristic of mesoporous materials.[30] The

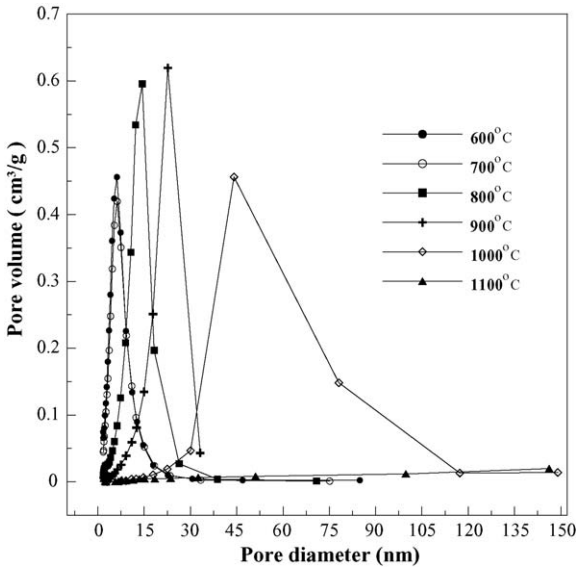

Fig. 4. BJH pore size distribution of YSZ powders calcined at various temperatures.

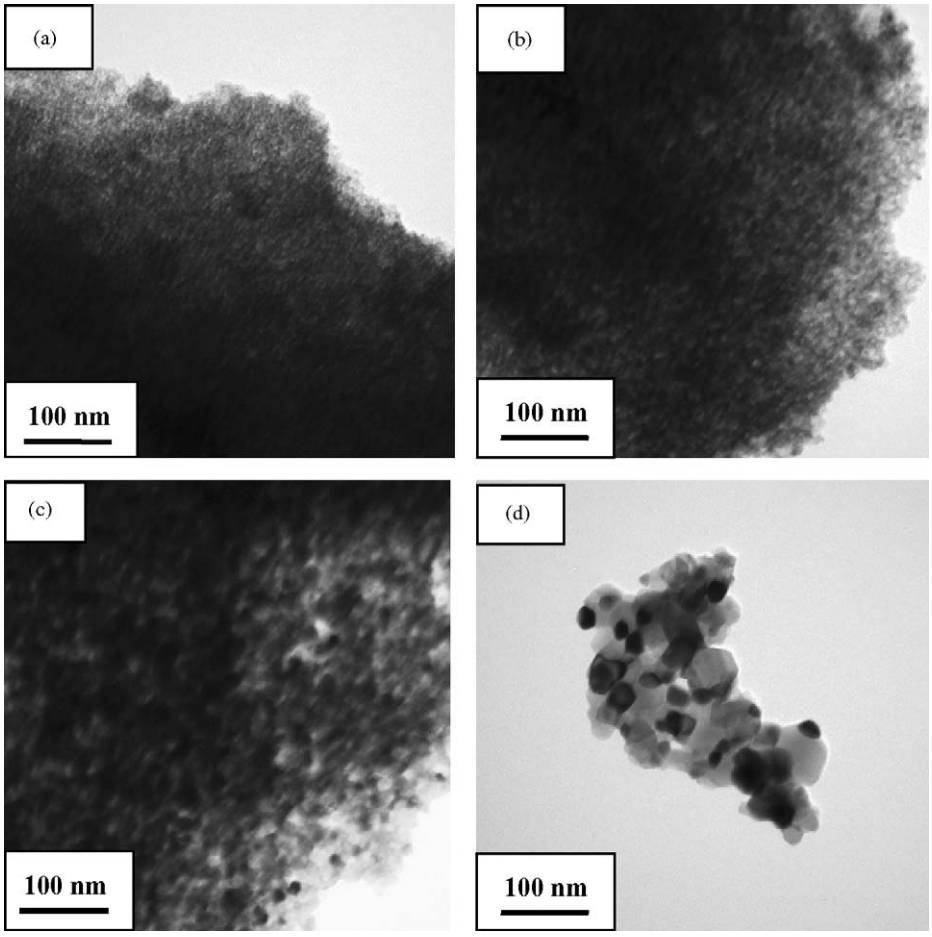

Fig. 5. TEM images of YSZ powders calcined at (a) 600 °C; (b) 700 °C; (c) 900 °C; and (d) 1000 °C.

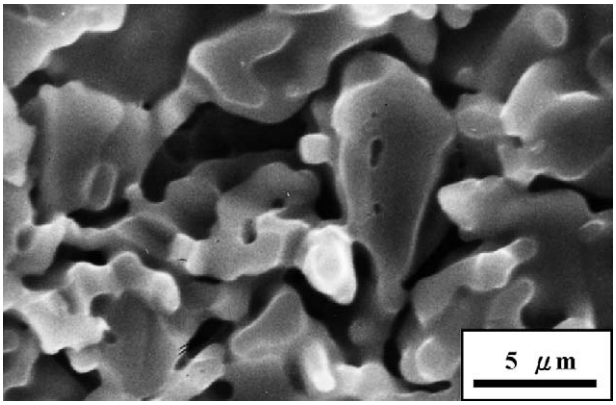

Fig. 6. The SEM micrograph of mesoporous YSZ as sintered at 1500 °C for 6 h.

Barrett–Joyner–Halender (BJH) pore distribution is narrow with a mean pore size at 5.0 nm. The mesoporous structure remain intact even the calcination temperature increased to 700 °C. Neither the shape of isotherm nor the distribution of pore size significantly alters. For instance, the BET surface area for mesoporous YSZ powders calcined at 600 °C was 137 m^2/g and the total pore volume as high as 0.21 cm^3/g. After calcining at 700 °C, the BET surface area and total pore volume slightly decreased to 124 m^2/g and 0.2 cm^3/g, respectively. For the sample calcination at 800 °C, the BET surface area rapidly decreased to 66 m^2/g and the hysteresis loop apparently shifted to higher pressure, indicating that the larger pore sizes formed. Such pores can be classified as the mixture of type H1 and type H2. The evolution of pore morphology is attributed to partial degradation of the walls surrounding meso-pores leading to an extended networking of pores. The mean pore diameter increased to 10 nm. As the calcination temperature increased to 900 °C, a similar isotherm was observed and the mean pore size increased to 17.4 nm. As the sample calcined at 1000 °C, the hysteresis loop was no longer observed and the BJH pore size distribution showed a broaden peak. Such a wide pore size distribution was caused by the collapse of the mesoporous structure and the subsequent formation of a bottleneck structure.

The evolution of mesoporous structure of YSZ was further examined by TEM. TEM images of mesoporous YSZ powders calcined at 600, 700 and 900 °C are shown in Fig. 5(a)–(c). The pore architecture of these samples is disordered "wormhole-like" variety.[15,32] The TEM image of YSZ powder calcined at 1000 °C is shown in Fig. 5(d). After calcining at 1000 °C, the average crystallite size was found to increase to ~35–65 nm and the mesoporous structure no longer observed.

From the SEM micrograph of sintered sample, as shown in Fig. 6, a porous networking microstructure was found. This porous YSZ exhibits a lot of open channels and the porosity as high as 33%. To the best of our knowledge, porous YSZ with porosity as high as 33% was first reported without adding any pore former, such as polymer or carbon. For the formation of low-densified YSZ samples from mesoporous YSZ powder, it may be concluded that the mesopores grew into large connected channel during calcination and sintering process. Then surface area energy of mesoporous YSZ powder was consumed at low temperature. Subsequently, these interconnected open channels prohibit the further densification of YSZ samples. Such an open structure may be used as the skeleton of SOFC electrodes in order to reduce the concentration polarization. Further coming, mesoporous Ni/YSZ anode cermet will be prepared by this method and its effect on the concentration polarization will be investigated.

4. Conclusions

The nanocrystalline mesoporous YSZ was successfully prepared using CTAB as the surfactant and urea as the hydrolyzing agent. Mesoporous YSZ exhibits high specific surface area of 137 m^2/g at 600 °C and highly stable mesoporous structure, in which the meso-pores can be retained up to 900 °C. The crystallite size of mesoporous YSZ in the range of 5.8–47.2 nm under the calcination temperatures ranging from 600 to 1200 °C. At high temperature, the meso-pores in YSZ grew into large connected channel. The surface area energy of mesoporous YSZ powder was consumed at low temperature. These interconnected open channels prohibit the further densification of YSZ sample.

Acknowledgment

The authors would like to acknowledge the financial support from the National Science Council of Taiwan under grant No. NSC-92-2120-M-006-004.

References

1. Minh, N. Q., Ceramic fuel cells. *J. Am. Ceram. Soc.*, 1993, **76**, 563–588.
2. Can, Z. Y., Narita, H., Mizusaki, J. and Tagawa, H., Detection of carbon monoxide by using zirconia oxygen sensor. *Solid State Ionics*, 1995, **79**, 344–348.
3. Dubbe, A., Fundamentals of solid state ionic micro gas sensors. *Sens. Actuators B*, 2003, **88**, 138–148.
4. Yao, H. C. and Yao, Y. F. Y., Ceria in automotive exhaust catalysts. I. Oxygen storage. *J. Catal.*, 1984, **86**, 254–265.
5. Kresge, C. T., Leonowicz, M. E., Roth, W. J., Vartuli, J. C. and Beck, J. S., Ordered mesoporous molecular sieves synthesized by a liquid-crystal template mechanism. *Nature*, 1992, **359**, 710–712.
6. Beck, J. S., Vartuli, J. C., Roth, W. J., Leonowicz, M. E., Kresge, C. T., Schmitt, K. D. *et al.*, A new family of mesoporous molecular sieves prepared with liquid crystal templates. *J. Am. Chem. Soc.*, 1992, **114**, 10834–10843.
7. Yang, P., Zhao, D., Margolese, D. I., Chmelka, B. F. and Stucky, G. D., Generalized syntheses of large-pore mesoporous metal oxides with semicrystalline frameworks. *Nature*, 1998, **396**, 152–155.
8. Coakley, K. M., Liu, Y., McGehee, M. D., Frindell, K. L. and Stucky, G. D., Infiltrating semiconducting polymers into self-assembled mesoporous titania films for photovoltaic applications. *Adv. Funct. Mater.*, 2003, **13**, 301–306.
9. Xu, X., Tian, B., Kong, J., Zhang, S., Liu, B. and Zhao, D., Ordered mesoporous niobium oxide film: a novel matrix for assembling functional proteins for bioelectrochemical applications. *Adv. Mater.*, 2003, **15**, 1932–1936.
10. Peng, Z., Shi, Z. and Liu, M., Mesoporous Sn–TiO_2 composite electrodes for lithium batteries. *Chem. Commun.*, 2000, **21**, 2125–2126.
11. Mamak, M., Coombs, N. and Ozin, G. A., Electroactive mesoporous yttria stabilized zirconia containing platinum or nickel oxide nanoclusters: a

new class of solid oxide fuel cell electrode materials. *Adv. Funct. Mater.*, 2001, **11**, 59–63.
12. Mamak, M., Coombs, N. and Ozin, G. A., Mesoporous nickel-yttria-zirconia fuel cell materials. *Chem. Mater.*, 2001, **13**, 3564–3570.
13. Mamak, M., Metraux, G. S., Petrov, S., Coombs, N., Ozin, G. A. and Green, M. A., Lanthanum strontium manganite/yttria-stabilized zirconia nanocomposites derived from a surfactant assisted, co-assembled mesoporous phase. *J. Am. Chem. Soc.*, 2003, **125**, 5161–5175.
14. Mamak, M., Coombs, N. and Ozin, G. A., Practical solid oxide fuel cells with anodes derived from self-assembled mesoporous-NiO-YSZ. *Chem. Commun.*, 2002, **20**, 2300–2301.
15. Teoh, L. G., Hung, I. M., Shieh, J., Lai, W. H. and Hon, M. H., High sensitivity semiconductor NO_2 gas sensor based on mesoporous WO_3 thin-films. *Electrochem. Solid-State Lett.*, 2003, **6**, G108–G111.
16. Cabot, A., Arbiol, J., Cornet, A., Morante, J. R., Chen, F. and Liu, M., Mesoporous catalytic filters for semiconductor gas sensors. *Thin Solid Films*, 2003, **436**, 64–69.
17. Sayari, A. and Liu, P., Non-silica periodic mesostructured materials: recent progress. *Microporous Mater.*, 1997, **12**, 149–177.
18. Schuth, F., Non-siliceous mesostructured and mesoporous materials. *Chem. Mater.*, 2001, **13**, 3184–3195.
19. Crepaldi, E. L., Soler-Illia, G. J., de, A. A., Grosso, D. and Sanchez, C., Nanocrystallised titania and zirconia mesoporous thin-films exhibiting enhanced thermal stability. *New J. Chem.*, 2003, **27**, 9–13.
20. Mamak, M., Coombs, N. and Ozin, G., Mesoporous yttria-zirconia and metal-yttria-zirconia solid solutions for fuel cells. *Adv. Mater.*, 2000, **12**, 198–202.
21. Mamak, M., Coombs, N. and Ozin, G., Self-assembling solid oxide fuel cell materials: mesoporous yttria-zirconia and metal-yttria-zirconia solid solutions. *J. Am. Chem. Soc.*, 2000, **122**, 8932–8939.
22. Chen, F. and Liu, M., Preparation of mesoporous yttria-stabilized zirconia (YSZ) and YSZ ± NiO using a triblock copolymer as surfactant. *J. Mater. Chem.*, 2000, **10**, 2603–2605.
23. Wang, Y., Yin, L., Palchik, O., Hacohen, Y. R., Koltypin, Y. and Gedanken, A., Sonochemical synthesis of layered and hexagonal yttrium-zirconium oxides. *Chem. Mater.*, 2001, **13**, 1248–1251.
24. Wang, Y. Q., Yin, L. X., Palchik, O., Hacohen, Y. R., Koltypin, Y. and Gedanken, A., Rapid synthesis of mesoporous yttrium-zirconium oxides with ultrasound irradiation. *Langmuir*, 2001, **17**, 4131–4133.
25. Souza, S., Visco, S. J. and Jonghe, L. C., Thin-film solid oxide fuel cell with high performance at low-temperature. *Solid State Ionics*, 1997, **98**, 57–61.
26. Virkar, A. V., Chen, J., Tanner, C. W. and Kim, J. W., The role of electrode microstructure on activation and concentration polarizations in solid oxide fuel cells. *Solid State Ionics*, 2000, **131**, 189–198.
27. Shaw, W. H. R. and Bordeaux, J. J., The decomposition of urea in aqueous media. *J. Am. Chem. Soc.*, 1955, **77**, 4729–4733.
28. Cullity, B. D., *Elements of X-ray Diffraction*. Addison-Wesley, California, 1978, pp. 284–285.
29. Kleitz, F., Schmidt, W. and Schuth, F., Evolution of mesoporous materials during the calcination process: structure and chemical. *Microporous Mesoporous Mater.*, 2001, **44–45**, 95–109.
30. Gregg, S. J. and Sing, K. S. W., *Adsorption Surface Area, and Porosity*. Academic Press Ltd., London, 1982, pp. 111–112.
31. Audebr, N., Auffredic, J. P. and Louer, D., An X-ray powder diffraction study of the microstructure and growth kinetics of nanoscale crystallites obtained from hydrated cerium oxides. *Chem. Mater.*, 2000, **12**, 1791–1799.
32. Hung, I. M., Wang, H. P., Lai, W. H., Fung, K. Z. and Hon, M. H., Preparation of mesoporous cerium oxide templated by tri-block copolymer for solid oxide fuel cell. *Electrochim. Acta*, 2004, **50**, 745–748.